Article

Flexible Ultraviolet Sensor Based on Zinc Oxide Nanoparticle Powder

Nicol Alejandra Munguía-Fernández [1], Jhonathan Rafael Castillo-Saenz [2], Oscar Manuel Perez-Landeros [2,*], Roumen Nedev [2], David Mateos [2], Judith Paz [2], Mariel Suárez [1], Mario Alberto Curiel-Alvarez [2], Nicola Nedev [2] and Abraham Arias [1,*]

[1] Facultad de Ingeniería, Universidad Autónoma de Baja California, Blvd. Benito Juárez s/n C.P., Mexicali 21280, Mexico
[2] Instituto de Ingeniería, Universidad Autónoma de Baja California, Blvd. Benito Juárez s/n C.P., Mexicali 21280, Mexico
* Correspondence: oscar.manuel.perez.landeros@uabc.edu.mx (O.M.P.-L.); arias.abraham@uabc.edu.mx (A.A.)

Abstract: Zinc oxide nanopowder was synthesized by the coprecipitation method. FT-IR and EDS analyses were performed to qualitatively determine the composition of the nanopowder. FE-SEM images revealed the morphology of the nanopowder formed by clusters of nanoparticles. An XRD analysis confirmed the wurtzite structure with a crystallite size of ~21.2 nm. UV–Vis measurements were performed to determine the ZnO bandgap (~3.05 eV) using the Tauc plot method in the absorbance spectra. The ZnO nanopowder and two comb-like metal contacts were confined and compacted between two polymeric layers by a low-temperature thermal lamination method, resulting in a flexible Polymer/ZnO/Metal/ZnO/Polymer structure. Part of each comb-like metal was kept uncovered by a polymeric layer in order to be used for electrical characterization. I-V measurements of the flexible structure were performed in the dark and under UV illumination, showing the capacity to detect UV radiation and its potential application as a visible-blind UV sensor. A facile and low-cost flexible optoelectronic device is presented, avoiding using high-vacuum or high-temperature technology. This new and novel approach to developing optoelectronic devices proposes using powder materials as semiconducting active regions instead of thin films; this could eliminate the cracking and delamination problems of flexible devices based on thin film technology.

Keywords: flexible electronics; nanopowder; UV sensor

1. Introduction

We can explore different areas and applications of the flexible electronics technology due to its compatibility with movable parts and arbitrarily curved surfaces [1], such as wearable sensors for health monitoring and optoelectronic devices [2]. The mechanical properties and transparency characteristics of flexible electronics have become a critical-improvement field. ZnO nanoparticles are part of deformable and bendable nanomaterials deposited on polymer substrates, employing different fabrication processes [2].

Devices for monitoring UV radiation can be beneficial in different applications such as communications, biomedical instrumentation, and high-temperature plasma research [3]. However, humans are susceptible to UV-A radiation which has a wavelength of 320–400 nm, and the constant exposure to UV-A radiation can cause health problems including premature aging and skin cancer. For these reasons, interest has been generated in UV photodetectors [4].

Zinc oxide (ZnO) is a transparent semiconductor oxide that has attracted considerable attention because of its electrical and optical properties and excellent chemical stability [5]. ZnO has a bandgap in the 3.0–3.4 eV range, depending on the synthesis method or the preparation parameters [6]. In addition, ZnO has applications in thin-film transistors [7],

gas sensors [8], the electron transport layer in solar cells [9], photocatalysis [10], Schottky barrier diodes [11], piezoelectric devices [12], and UV detectors [13].

The crystalline wurtzite structure is present in zinc oxide. Recently, studies have been conducted by applying the density functional theory (DFT) to treat structural formations by clusters or nanoparticles of materials that exhibit the wurtzite structure [14]. Nowadays, the developed DFT models are in accordance with experimental data and can be used for guidance before an experimental work.

ZnO has been synthesized using various methods. However, some of the synthesis methods are expensive and/or require ultrahigh vacuum environments, for example, RF sputtering [15], PLD [16], CVD [17], or ALD [18]. Low-cost chemical-based alternatives, such as hydrothermal methods [19], colloidal synthesis [20], sol-gel [21], and precipitation methods [22], have been proposed for zinc oxide. The precipitation method is an effective and simple technique for obtaining zinc oxide nanopowders.

Several forms of ZnO nanostructures have been synthesized, grown, or deposited in the development of UV photosensors in recent years [13], mainly nanoparticles, quantum dots, nanowires, nanorods, nanofibers, nanobelts, and nanosheets [13]. Different alternatives have been tried in the quest to improve UV photodetectors, such as hybrid heterojunctions of organic and inorganic materials including polypyrrole and gallium nanorods [4] or p-type polymers and n-type ZnO nanorods combining its different physics properties [23]. Also, an n-type ZnO layer has been used on a different-wavelengths photodetector in order to enhance the charge transfer efficiency of the heterostructure [24].

Additionally, a few studies based on zero-dimensional ZnO nanoparticles have yielded a better result of absorption efficiency compared to other dimensional structures [25]. UV photosensors have been reported as either rigid or flexible devices. Flexible substrates include polyimide for flexible packages and as a dielectric interlayer in integrated circuits; Kapton, which for its high-temperature resistance and chemical stability, is used for tactile sensors [26,27]; paper for environmental monitoring and as a potential application as printed circuit board in optoelectronics employing sublimated copper phthalocyanine with organic thin films to reduce its capillarity [28]; PET used to create flexible circuitry, where it is important to maintain thermal stability [29]; and PDMS, which is already used to fabricate UV photodetectors due to its facile fabrication process and great flexibility [30]; these are now are being used to fabricate bendable photodetectors, incorporating the lamination process to combine materials together [2,31].

This study presents a novel approach to developing UV sensors based on ZnO. For the first time, ZnO nanopowders are mechanically confined and compacted between two polymeric layers by a low-temperature thermal lamination method. The metal contacts of the resulting flexible sensor are also confined during the one-step thermal lamination process. A facile and low-cost flexible optoelectronic device is presented, avoiding using high-vacuum or high-temperature technology.

2. Materials and Methods

2.1. ZnO Nanopowder Synthesis

A precursor solution of 0.5 M Zn^{2+} was prepared by dissolving 5.49 g of zinc acetate dehydrate [Zn $(CH_3COO)_2 \bullet 2H_2O$] (Sigma-Aldrich, Burlington, NJ, USA) in 50 mL of deionized water. The pH was adjusted to 14 by adding 0.5 M sodium hydroxide (NaOH) solution drop-to-drop in constant agitation. Vacuum filtration was used to separate the zinc hydroxide [$Zn(OH)_2$] precipitates formed from the mother liquor. $Zn(OH)_2$ was washed with deionized water several times and dried at 80 °C for 12 h. Finally, $Zn(OH)_2$ was calcined at 400 °C in a muffle furnace for two hours in the air to obtain ZnO nanopowder.

2.2. ZnO Nanopowder Characterization

The morphology and elemental composition of ZnO nanopowder were studied using a field emission scanning electron microscope FE-SEM Lyra 3 XMU (Tescan, Brno–Kohoutovice, Brno, Czech Republic), equipped with an energy-dispersive X-ray detector

(EDS). Structural and crystallographic information was obtained by X-ray diffraction (XRD) analysis using a PANalytical Empyrean diffractometer with a Cu Kα radiation source (λ = 0.15406 nm) and a real-time multipass detector X'Celerator. The ZnO nanopowder was scanned over a 2θ range of 20–80°. Fourier transform infrared (FT-IR) spectra were recorded in the 500–4000 cm^{-1} range using a Frontier FT-IR (PerkinElmer, Shelton, WD, USA) instrument in the attenuated total reflection mode. The UV-Vis absorption spectrum was measured in the 300–800 nm range using a Cary model 50 spectrometer (Varian, Mulgrave, Australia).

2.3. Sensor Development

A flexible UV radiation sensor based on ZnO nanopowder was designed and fabricated. The device was embedded between two transparent flexible polymer films. The final device is shown in Figure 1a. The geometries of the top and bottom polymer films and the Cu electrodes were obtained via a micromachining process. The process is described next, and the dimensions are shown in Figure 1b. The bottom mica substrate was trenched at a 40 μm depth to leave space between the Cu electrodes and the top mica sheet. The Cu electrodes were milled as comb-like structures with two and three fingers. The comb electrodes were embedded in ZnO nanopowder, and the powder was confined mechanically in a volume of 4.6 × 3.9 × 0.04 (x, y, z) millimeters, such that it had free movement over, under, and between the fingers of the Cu comb electrodes. Then, it was finally sealed via a thermal lamination process at 120 °C.

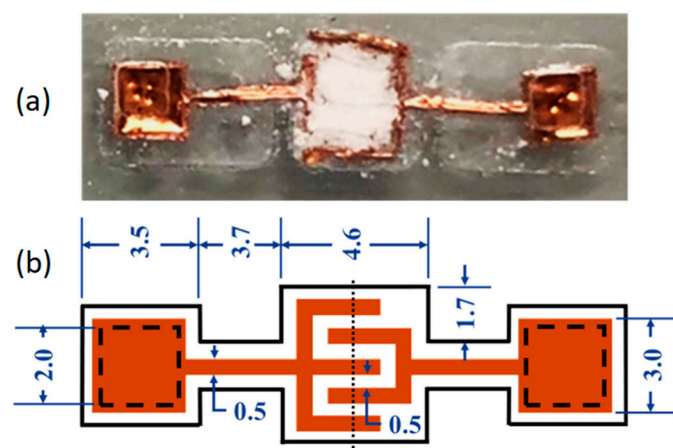**Figure 1.** Flexible nanopowder-based UV radiation sensor (**a**) and scheme with dimensions in millimeters (**b**).

3. Results and Discussion

The SEM images in Figure 2 show the morphology of the nanopowder formed by clusters (Figure 2a) of ZnO nanoparticles with dimensions between 20 and 50 nm (Figure 2b). The SEM images were taken with an acceleration voltage of 10 kV and an optimal working distance of 9 mm. The chemical composition of the ZnO nanopowder was qualitatively determined using EDS. Only Zn and O were detected in the synthesized material (Figure 2c), showing that a high-purity material was obtained; no contaminants were detected. The EDS analysis was carried out under the same SEM conditions, with an acquisition time of 1 min.

The XRD results for ZnO nanopowder are shown in Figure 3. The peaks in Figure 3 at 2θ = 31.9°, 34.5°, 36.35°, 47.6°, 56.6°, 62.9°, 66.4°, 67.9°, 69.2°, 72.6°, and 77.0° correspond to (100), (002), (101), (102), (110), (103), (200), (112), (201), (004), and (202) planes, respectively. These peaks correspond to the typical signals of ZnO and confirm the formation of the wurtzite structure with a hexagonal phase, according to (JCPDS card no. 36–1451) and pre-

viously published studies [4,32]. Table 1 shows the crystallite size of the ZnO nanopowder calculated using the Scherrer equation:
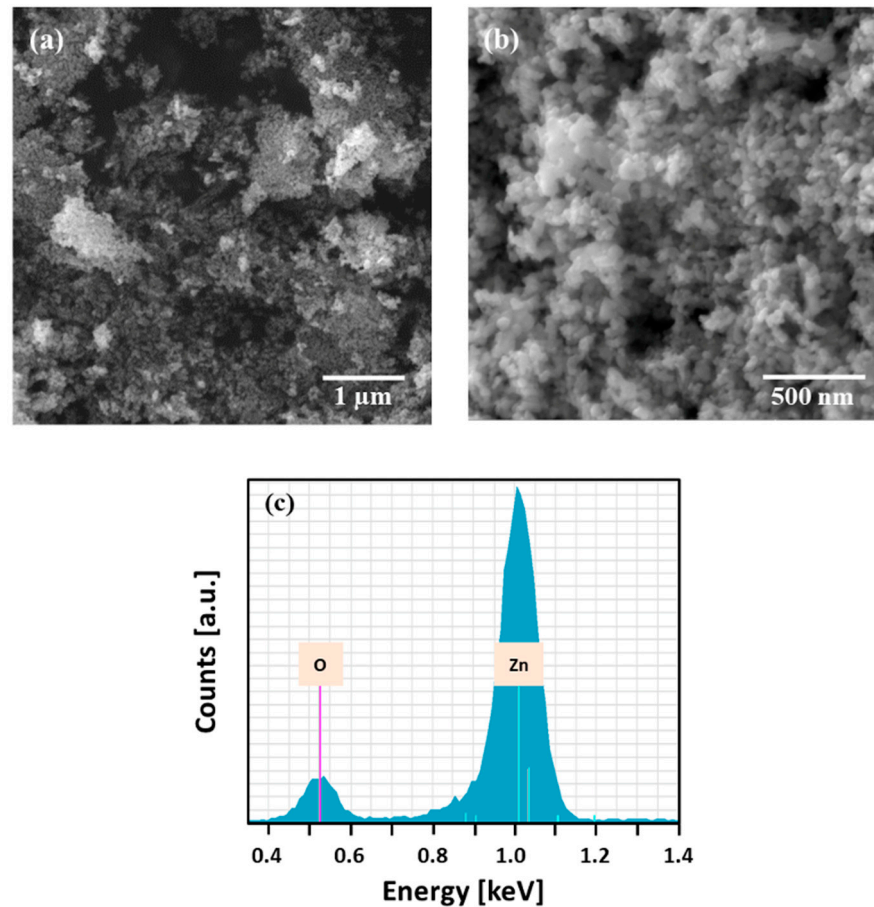
$$D = \frac{0.89\lambda}{\beta cos\theta}$$
(1)

Figure 2. SEM image of ZnO nanopowder, magnification of (**a**) 40 kx and (**b**) 100 kx, respectively, and (**c**) EDS spectra of ZnO nanopowder.
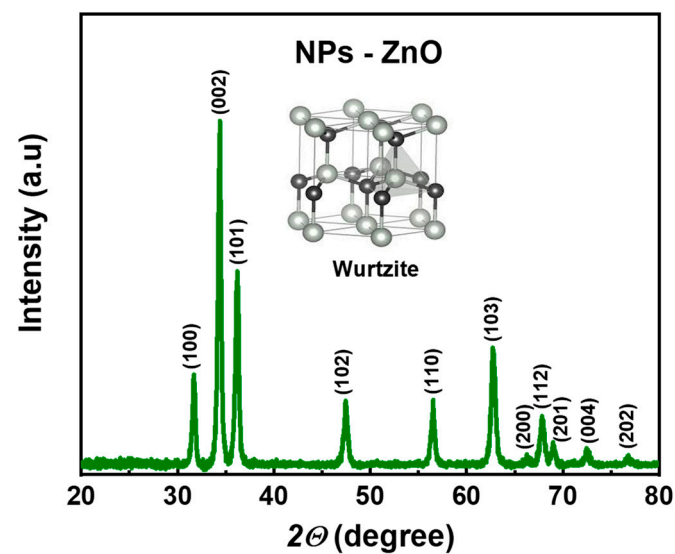

Figure 3. XRD patterns of ZnO nanopowder.

Table 1. ZnO crystallite size obtained by Scherrer equation.

2θ (°)	FWHM	(*hkl*)	Crystallite Size (nm)
34.39	0.387	(002)	~21.2

Here, D is the crystallite size, λ is the X-ray wavelength, β is the full width at half maximum (FWHM) of the most intense peak, and θ is the Bragg angle in radians.

The FT-IR spectrum (Figure 4) exhibited one characteristic peak at 510 cm^{-1}, corresponding to the Zn–O stretching vibrational mode [22]. The infrared spectrum showed no absorption in the 3200–3650 cm^{-1} region, which indicates that the synthesized material was free of O–H groups.
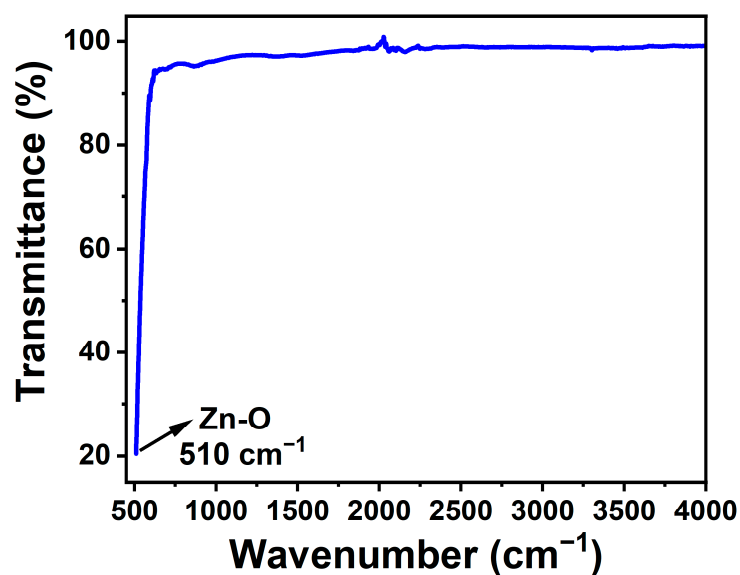
Figure 4. FT-IR spectrum of ZnO nanopowder.

The UV-Vis spectrum is shown in Figure 5. The optical bandgap of the ZnO was estimated by the Tauc plot method from the absorption measurements. The Tauc expression relates optical bandgap, E_g, and absorption coefficient, α, by the following expression

$$\alpha h\nu = B\left[(h\nu - E_g)\right]^n \tag{2}$$

where $h\nu$ is the photon energy, and n is a number that depends on the nature of the electronic transitions responsible for the absorption. For a semiconductor with a direct bandgap, which is the case for ZnO, n equals 2 [33]. E_g was determined by fitting the linear part of $(\alpha h\nu)^2$ vs. $h\nu$ dependence, extrapolated to the energy axis (inset Figure 5). The optical band gap obtained for ZnO was ~3.05 eV.

The electrical characterization of the ZnO nanopowder-based flexible UV sensor was performed using a Keitlhey 2400-C Source Monitor Unit with 4-wire configuration at ambient temperature. The GUI used was the "I-V Measurements" developed by Dr Michael Kelzenberg. The UV source was a typical 5 mm UV LED with a wavelength centered at 395 nm. The optical power of the UV source was measured with a Thorlabs (Newton, NJ, USA) PMUSB100 Power Meter with a Thorlabs S120VC Sensor (Si Photodiode UV Extended) in a 200 to 800 nm range. The software used was the "Optical Power Monitor" from Thorlabs. The optical power for every wavelength is shown in Figure 6. The spectral region of the UV source that is positioned to the left of the blue line in Figure 6 is potentially detectable by the proposed UV sensor. The optical power density of the UV source at 395 nm was 120 mW/cm^2. The distance between the UV sensor and all the illumination sources was 50 mm.
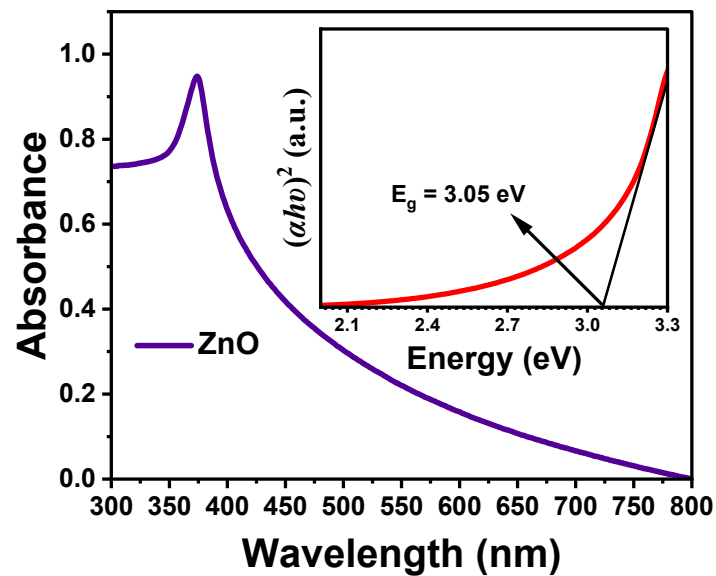
Figure 5. UV-Vis spectrum of ZnO nanopowder; inset. Optical bandgap energy (E_g) for ZnO determined from Tauc model.
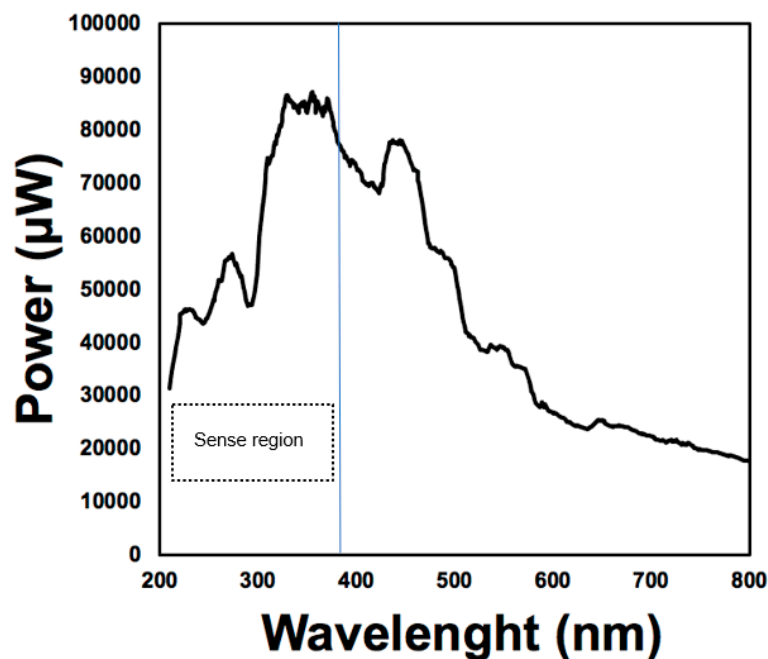

Figure 6. Optical power of UV source in a 200–800 nm range.

The I-V characteristics of the flexible UV photosensor in the dark and under red, green, blue, and UV illumination are depicted in Figure 7. The curves obtained under red-, green-, and blue-light illumination coincide with the dark current. The purple line represents the electrical characteristic of the sensor under UV radiation. Figure 8 shows the I_{on}/I_{off} ratio in the 0 to ± 10 V range reaching values of $\sim 3.2 \times 10^1$. In Figure 9, the rectification ratio of the sample was measured, obtaining a constant value of ~1.25 in the entire range. The UV-Vis (red, green, blue) rejection ratio is depicted in Figure 10. At -10 V for the three different visible sources, the rejection ratio was ~35.
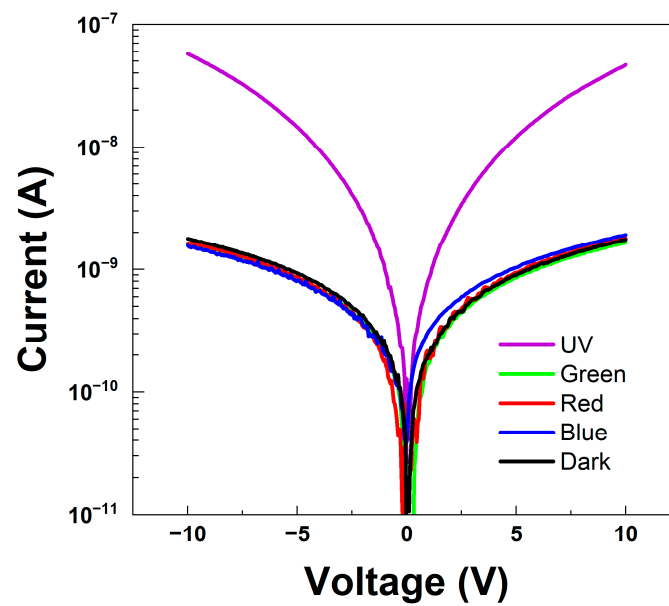
Figure 7. I-V dependencies in the dark and under red, green, blue, and UV illumination of the flexible UV sensor.
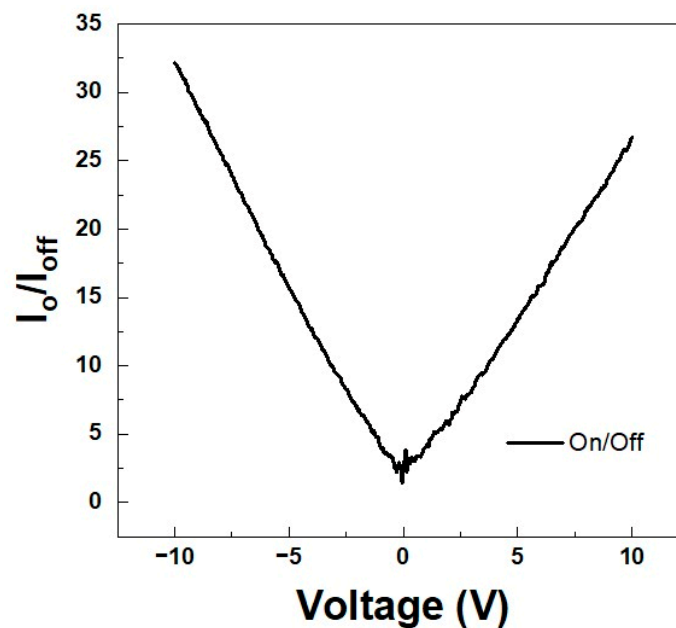

Figure 8. I_{on}/I_{off} ratio in the 0 to ± 10 V range of the flexible UV sensor.

The measurements shown in Figure 11 were performed from 0 V to 5 V in the dark and then from 0 V to 5 V under UV illumination. The same alternating Dark/UV measurements were performed from 0 V to 6, 7, 8, 9, and 10 V in the forward direction. The same order of measurements was subsequently performed in the negative direction. At any voltage and in any direction, the amount of measured current was higher under UV illumination than in the dark, showing the capacity of this flexible structure to sense UV irradiation. The measured current under UV illumination was ~20 times higher in the forward direction and ~30 times higher in the negative direction than the dark current.
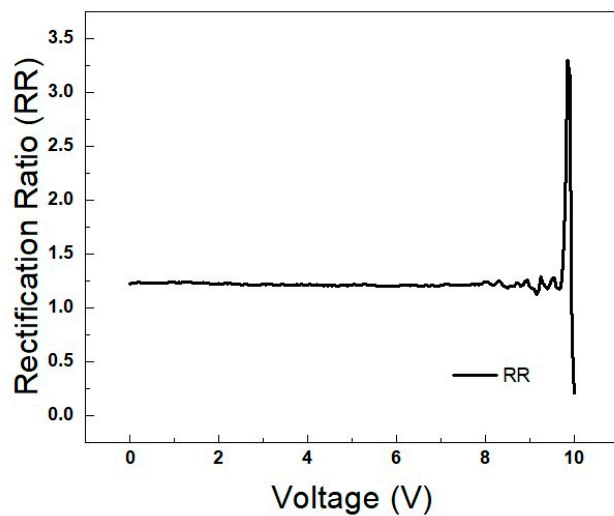
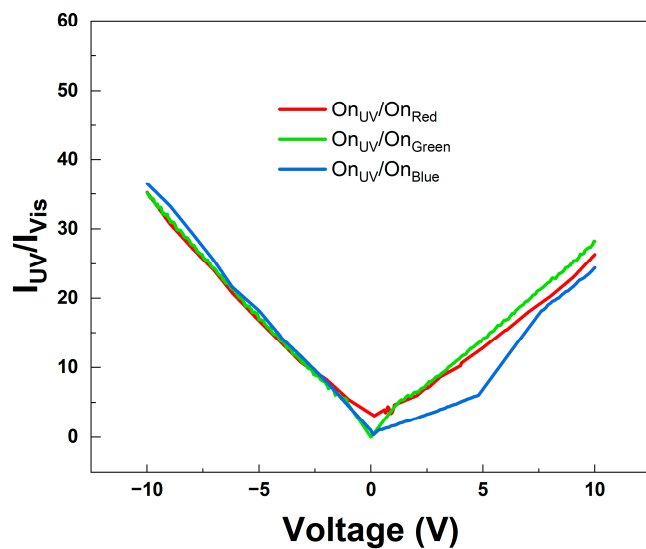**Figure 9.** Rectification ratio in the 0 to ±10 V range of the flexible UV sensor.

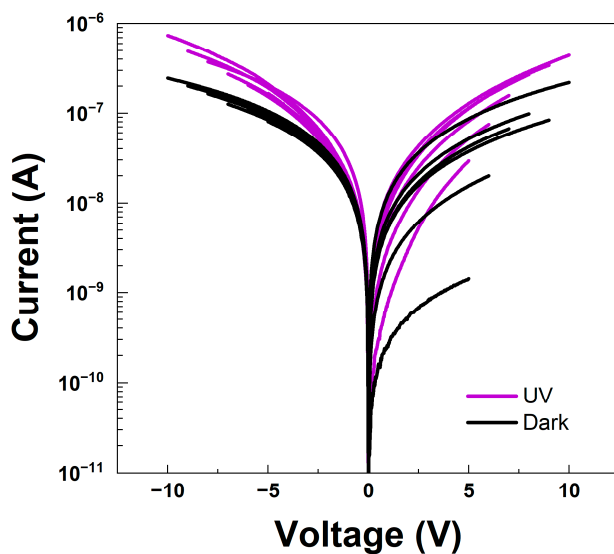**Figure 10.** UV-Vis rejection ratio for the UV flexible sensor.

Figure 11. I-V dependencies in the dark and under UV illumination of the flexible UV sensor.

The differences in the slope shape and the current values of measurements carried out in the two directions are due to an instrumentation effect. This asymmetric behavior results from the setup of the probe station and the internal variations of the SMU and GND modules. When the measurement probes or the modules configuration were interchanged, a mirror graph similar to the one on Figure 11 was obtained; this effect was previously reported in Ref. [34]. Since the ZnO nanopowder was confined between two transparent polymer films, experiments with the illumination source placed in two different positions, at the top and bottom of the sensor, were carried out. There was no significant difference in the results obtained when the illumination source position was changed, revealing that the shadowing effect can be neglected in the comb-like electrodes. However, these results also reveal that the confined nanopowder acts like a whole active region despite its powder nature. A slight difference in the curve slope exists between the measurements performed at 5 V compared to 10 V. It is assumed that this behavior is due to an electrical charge trapped in the interfacial regions between the ZnO nanoparticles.

Figure 12 shows the electrical characteristics of the flexible UV sensor when the measurements are alternated between forward and negative directions. The measurements were performed as follows: first from 0 V to 5 V in the dark and then from 0 V to 5 V under UV illumination. After that, the measurements were performed in the negative direction from 0 V to -5 V in the dark and then from 0 V to -5 V under UV. The alternating Forward/Negative direction measurements were performed in the ranges of 0 V to ± 6, ± 7, ± 8, ± 9, and ± 10 V. In Figure 12, it can be observed that when the measurement directions are alternated, the slopes of the I-V curves under UV illumination remain almost the same. In addition, the amount of current at the forward and negative voltages under illumination is practically the same. Also, the magnitude of the dark currents for all ranges of voltages is nearly constant. There is a slightly difference in the slope shape of the dark current with a variation in the voltage range. This behavior could be associated with a process of charge/discharge in the interfaces of the nanoparticles of the ZnO nanopowder derived from the change in the measurement direction. The shape of the I-V curves in Figure 11 could be associated with the accumulated charge in the ZnO nanopowder when all the measurements are performed in only one direction.
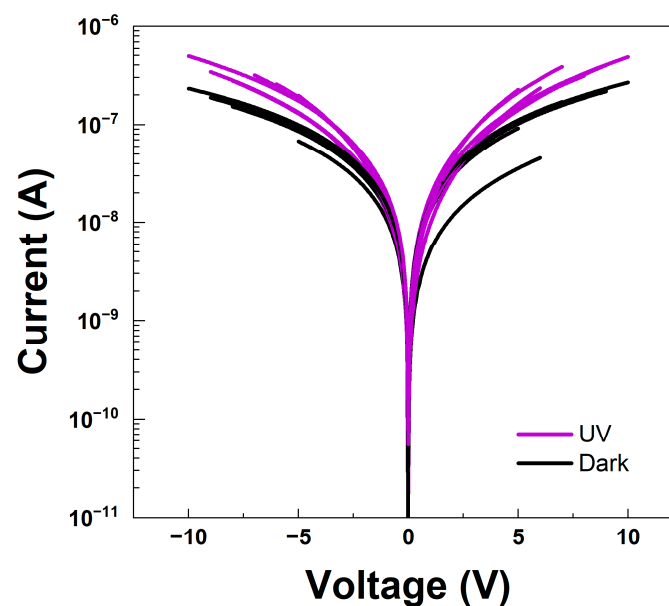

Figure 12. I-V dependencies in the dark and under UV illumination when the measurement directions are alternated between forward and negative directions.

Voltage sweeps under UV illumination were performed from 0 V to 5, 6, 7, 8, 9, and 10 V; between every measurement, voltage sweeps from 0 V to -10 V in the dark were

carried out to determine if the voltage of -10 V in the opposite direction had an effect on the electrical behavior of the sensor. All these measurements are depicted in Figure 13. The same set of measurements, but in different directions, were performed, and the results are presented in Figure 14.
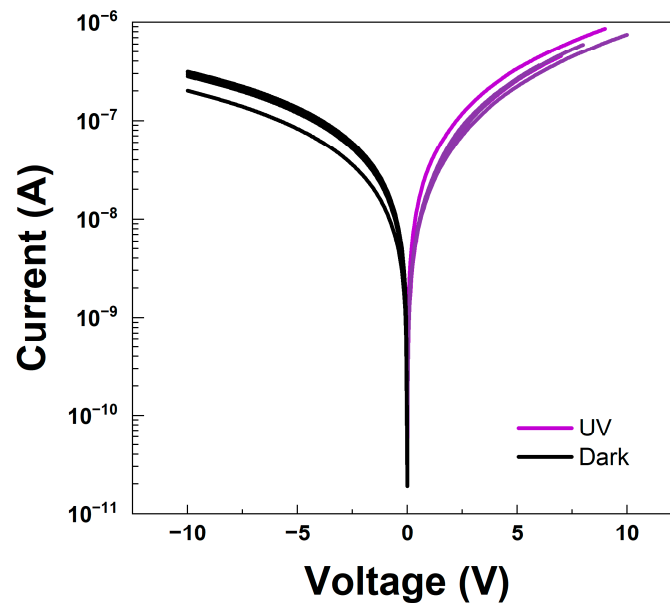

Figure 13. I-V dependencies of the flexible UV sensor using positive voltages under UV illumination and a discharge voltage sweep from 0 V to -10 V in the dark.
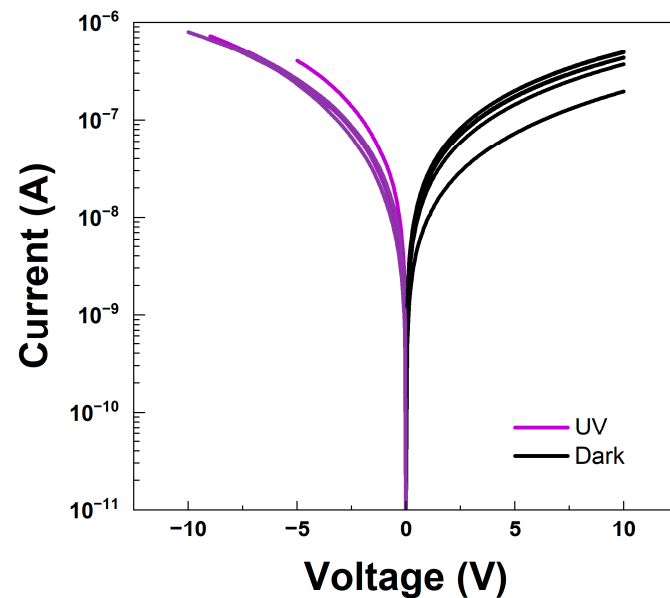

Figure 14. I-V dependencies of the flexible UV sensor using negative voltages under UV illumination and a discharge voltage sweep from 0 V to 10 V in the dark.

In Figure 13, it can be observed that the 0 V to -10 V discharge voltage-sweep improves the performance of the forward I-V characteristics under UV illumination, reducing the variation in the currents in comparison to Figures 11 and 12.

The best results of the proposed UV sensor were obtained when the UV sensing was performed using negative voltages and a 0 V to 10 V voltage-sweep in the dark as a discharge voltage; these results are shown in Figure 14. The I-V curves obtained under UV illumination overlap independently of the voltage range of the measurement; this behavior

is attributed to a discharge process due to the 0V to 10V measurement. A variation in the current can be observed in the measurements performed in the dark; this variation can be neglected since the voltage sweep is used only for discharging the UV sensor. The proposed sensor has to be discharged before every measurement with a sweep voltage in the opposite direction to that of the measurement.

The UV flexible sensor was subjected to bending cycles. The sensor was positioned in a bending machine where one side of the sensor was fixed to a stationary part and another side was attached to a moving part. The bending cycle consisted of a moving part that moved back and forth, achieving a bend with a ratio of ~3.1 mm, as can be observed in Figure 15. I-V measurements under UV radiation and in the dark were carried out after 200, 400, 600, 800, 1000, and 2000 cycles. The I-V characteristics after the bending cycles are shown in Figure 16; as was expected, the current measured under UV was always larger than the dark current. After every 200 bending cycles, an increment in the current can be observed. This increment is attributed to trapped charges in the ZnO. In the curve corresponding to 2000 bending cycles, a decrease in the current can be observed; this is attributed to the time elapsed between the measurement after 1000 bending cycles and the 2000 bending cycles. When a large amount of time is elapsed between measurements, the current value decreases due to a discharge process in the sensor over time.
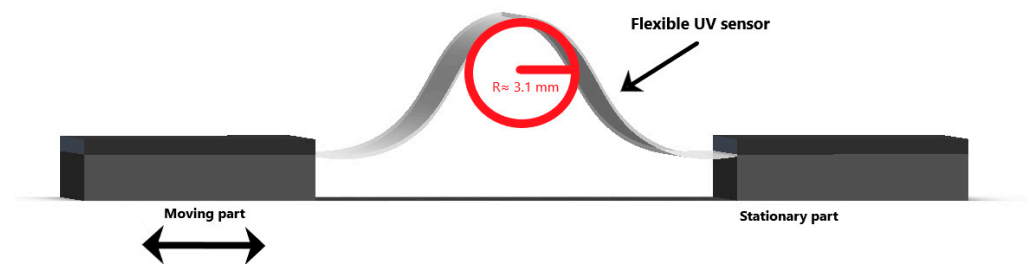

Figure 15. Schematic of the bending system for flexible electronic devices.
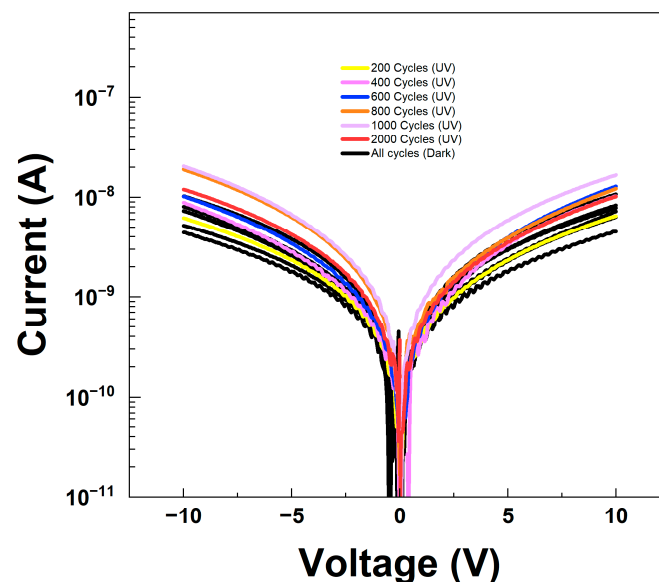

Figure 16. I-V dependencies of the flexible UV sensor under UV illumination and in the dark after bending cycles.

A further study of the effect of temperature on the electrical characteristics and of the nanoparticle size on the trapped charge has to be carried out. However, the trapped charge does not affect the ability of the structure to detect UV radiation.

4. Conclusions

ZnO powder was synthesized by the coprecipitation method. The composition purity was qualitatively determined by FT-IR and EDS analyses. FE-SEM images revealed the morphology of the nanopowder formed by clusters of nanoparticles. An XRD analysis revealed the wurtzite structure of the nanoparticles with a crystallite size of ~21.2 nm. The calculated ZnO bandgap was ~3.05 eV, using the Tauc plot method in the absorbance spectra. A facile and low-cost ZnO-nanopowder-based flexible UV sensor was designed and developed successfully at a low temperature via a thermal lamination process. The electrical measurements under UV illumination showed that the ZnO-nanopowder-based flexible sensor is an excellent candidate for UV sensing, even after several bending cycles. This work explores a new and novel approach to developing optoelectronic devices, proposing powder materials as semiconducting active regions instead of the thin films traditionally used in electronic applications. This new approach could eliminate the cracking and delamination problems of flexible devices based on thin film technology.

References

1. Han, S.T.; Peng, H.; Sun, Q.; Venkatesh, S.; Chung, K.S.; Lau, S.C.; Zhou, Y.; Roy, V.A.L. An overview of the development of flexible sensors. *Adv. Mater.* **2017**, *29*, 1700375. [CrossRef] [PubMed]
2. Cai, S.; Xu, X.; Yang, W.; Chen, J.; Fang, X. Materials and designs for wearable photodetectors. *Adv. Mater.* **2019**, *31*, 1808138. [CrossRef] [PubMed]
3. Panda, S.K.; Jacob, C. Preparation of transparent ZnO thin films and their application in UV sensor devices. *Solid State Electron.* **2012**, *73*, 44–50. [CrossRef]
4. Pasupuleti, K.S.; Reddeppa, M.; Park, B.G.; Oh, J.E.; Kim, S.G.; Kim, M.D. Efficient Charge Separation in Polypyrrole/GaN-Nanorod-Based Hybrid Heterojunctions for High-Performance Self-Powered UV Photodetection. *Phys. Status Solidi Rapid Res. Lett.* **2021**, *15*, 2000518. [CrossRef]
5. Tsay, C.Y.; Fan, K.S.; Lei, C.M. Synthesis and characterization of sol–gel derived gallium-doped zinc oxide thin films. *J. Alloys Compd.* **2012**, *512*, 216–222. [CrossRef]
6. Kumar, M.; Patel, M.; Nguyen, T.T.; Kim, J.; Yi, J. High-performing ultrafast transparent photodetector governed by the pyro–phototronic effect. *Nanoscale* **2018**, *10*, 6928–6935. [CrossRef]
7. Castillo-Saenz, J.R.; Nedev, N.; Martinez-Guerra, E.; Valdez-Salas, B.; Mendivil-Palma, M.I.; Curiel-Alvarez, M.A.; Hernández-Como, N. Bias-stress instabilities in low-temperature thin-film transistors made of Al_2O_3 and ZnO films deposited by PEALD. *Microelectron. Eng.* **2022**, *259*, 111788. [CrossRef]
8. Kumar, R.; Al-Dossary, O.; Kumar, G.; Umar, A. Zinc oxide nanostructures for NO_2 gas–sensor applications: A review. *Nanomicro Lett.* **2015**, *7*, 97–120. [CrossRef]
9. Zheng, D.; Wang, G.; Huang, W.; Wang, B.; Ke, W.; Logsdon, J.L.; Wang, H.; Wang, Z.; Zhu, W.; Yu, J.; et al. Combustion synthesized zinc oxide electron-transport layers for efficient and stable perovskite solar cells. *Adv. Funct. Mater.* **2019**, *29*, 1900265. [CrossRef]
10. Bica, B.O.; de Melo, J.V.S. Concrete blocks nano-modified with zinc oxide (ZnO) for photocatalytic paving: Performance comparison with titanium dioxide (TiO_2). *Constr. Build. Mater.* **2020**, *252*, 119120. [CrossRef]
11. Georgiadou, D.G.; Semple, J.; Sagade, A.A.; Forstén, H.; Rantakari, P.; Lin, Y.H.; Alkhalil, F.; Seitkhan, A.; Loganathan, K.; Faber, H.; et al. 100 GHz zinc oxide Schottky diodes processed from solution on a wafer scale. *Nat. Electron.* **2020**, *3*, 718–725. [CrossRef]
12. Bhadwal, N.; Ben Mrad, R.; Behdinan, K. Review of Zinc Oxide Piezoelectric Nanogenerators: Piezoelectric Properties, Composite Structures and Power Output. *Sensors* **2023**, *23*, 3859. [CrossRef] [PubMed]

13. Boruah, B.D. Zinc oxide ultraviolet photodetectors: Rapid progress from conventional to self-powered photodetectors. *Nanoscale Adv.* **2019**, *1*, 2059. [CrossRef] [PubMed]

14. Dos Santos, R.B.; Rivelino, R.; Gueorguiev, G.K.; Kakanakova-Georgieva, A. Exploring 2D structures of indium oxide of different stoichiometry. *CrystEngComm* **2021**, *23*, 6661. [CrossRef]

15. Ellmer, K. Magnetron sputtering of transparent conductive zinc oxide: Relation between the sputtering parameters and the electronic properties. *J. Phys. D Appl. Phys.* **2000**, *33*, R17–R32. [CrossRef]

16. Villanueva, Y.Y.; Liu, D.R.; Cheng, P.T. Pulsed laser deposition of zinc oxide. *Thin Solid Films* **2006**, *501*, 366–369. [CrossRef]

17. Waugh, M.R.; Hyett, G.; Parkin, I.P. Zinc oxide thin films grown by aerosol assisted CVD. *Chem. Vap. Depos.* **2008**, *14*, 366–372. [CrossRef]

18. Castillo-Saenz, J.R.; Nedev, N.; Valdez-Salas, B.; Martinez-Puente, M.A.; Aguirre-Tostado, F.S.; Mendivil-Palma, M.I.; Mateos, D.; Curiel-Álvarez, M.A.; Pérez-Landeros, O.; Martinez-Guerra, E. Growth of ZnO thin films at low temperature by plasma enhanced atomic layer deposition using H_2O and O_2 plasma oxidants. *J. Mater. Sci. Mater. Electron.* **2021**, *32*, 20274–20283. [CrossRef]

19. Mohan, S.; Vellakkat, M.; Aravind, A.; Reka, U. Hydrothermal synthesis and characterization of Zinc Oxide nanoparticles of various shapes under different reaction conditions. *Nano Express* **2020**, *1*, 030028. [CrossRef]

20. Van Embden, J.; Gross, S.; Kittilstved, K.R.; Della Gaspera, E. Colloidal Approaches to Zinc Oxide Nanocrystals. *Chem. Rev.* **2023**, *123*, 271–326. [CrossRef]

21. Davis, K.; Yarbrough, R.; Froeschle, M.; White, J.; Rathnayake, H. Band gap engineered zinc oxide nanostructures via a sol–gel synthesis of solvent driven shape controlled crystal growth. *RSC Adv.* **2019**, *9*, 14638. [CrossRef] [PubMed]

22. Uribe-López, M.C.; Hidalgo-López, M.C.; López-González, R.; Frías-Márquez, D.M.; Núñez-Nogueira, G.; Hernández-Castillo, D.; Alvarez-Lemus, M.A. Photocatalytic activity of ZnO nanoparticles and the role of the synthesis method on their physical and chemical properties. *J. Photochem. Photobiol. A Chem.* **2021**, *404*, 112866. [CrossRef]

23. Belhaj, M.; Dridi, C.; Yatskiv, R.; Grym, J. The improvement of UV photodetection based on polymer/ZnO nanorod heterojunctions. *Org. Electron.* **2020**, *77*, 105545. [CrossRef]

24. Wang, H.; Li, Z.; Li, D.; Chen, P.; Pi, L.; Zhou, X.; Zhai, T. Van der Waals integration based on two-dimensional materials for high-performance infrared photodetectors. *Adv. Funct. Mater.* **2021**, *31*, 2103106. [CrossRef]

25. Jun, J.H.; Seong, H.; Cho, K.; Moon, B.M.; Kim, S. Ultraviolet photodetectors based on ZnO nanoparticles. *Ceram. Int.* **2009**, *35*, 2797–2801. [CrossRef]

26. Dobrzynska, J.A.; Gijs, M.A. Flexible polyimide-based force sensor. *Sens. Actuators A Phys.* **2012**, *173*, 127–135. [CrossRef]

27. Deng, W.; Jin, L.; Zhang, B.; Chen, Y.; Mao, L.; Zhang, H.; Yang, W. A flexible field-limited ordered ZnO nanorod-based self-powered tactile sensor array for electronic skin. *Nanoscale* **2016**, *8*, 16302–16306. [CrossRef]

28. Domínguez, M.A.; Sosa-Sánchez, J.L. Copper phthalocyanine buffer interlayer film incorporated in paper substrates for printed circuit boards and dielectric applications in flexible electronics. *Solid State Electron.* **2020**, *172*, 107898. [CrossRef]

29. MacDonald, W.A.; Looney, M.K.; MacKerron, D.; Eveson, R.; Adam, R.; Hashimoto, K.; Rakos, K. Latest advances in substrates for flexible electronics. In *Large Area and Flexible Electronics*; Wiley: Hoboken, NJ, USA, 2015; pp. 291–314.

30. Albiss, B.A.; AL-Akhras, M.A.; Obaidat, I. Ultraviolet photodetector based on ZnO nanorods grown on a flexible PDMS substrate. *Int. J. Environ. Anal. Chem.* **2015**, *95*, 339–348. [CrossRef]

31. Qin, L.; Mawignon, F.J.; Hussain, M.; Ange, N.K.; Lu, S.; Hafezi, M.; Dong, G. Economic friendly ZnO-based UV sensors using hydrothermal growth: A review. *Materials* **2021**, *14*, 4083. [CrossRef]

32. Preethi, S.; Abarna, K.; Nithyasri, M.; Kishore, P.; Deepika, K.; Ranjithkumar, R.; Bhuvaneshwari, V.; Bharathi, D. Synthesis and characterization of chitosan/zinc oxide nanocomposite for antibacterial activity onto cotton fabrics and dye degradation applications. *Int. J. Biol. Macromol.* **2020**, *164*, 2779–2787. [CrossRef] [PubMed]

33. Patrycja, M.; Michal, P.; Wojciech, M. How to correctly determine the band gap energy of modified semiconductor photocatalysts based on UV–Vis spectra. *J. Phys. Chem. Lett.* **2018**, *9*, 6814–6817.

34. Arias, A.; Nedev, N.; Ghose, S.; Rojas-Ramirez, J.S.; Mateos, D.; Curiel Alvarez, M.; Droopad, R. Structural, optical, and electrical characterization of β-Ga_2O_3 thin films grown by plasma-assisted molecular beam epitaxy suitable for UV Sensing. *Adv. Mater. Sci. Eng.* **2018**, *2018*, 9450157. [CrossRef]